Climate Dynamics (2006) 26: 531–547
DOI 10.1007/s00382-005-0083-7

C. Caminade · L. Terray · E. Maisonnave

West African monsoon response to greenhouse gas and sulphate aerosol forcing under two emission scenarios

Received: 11 June 2004 / Accepted: 6 October 2005 / Published online: 14 January 2006

Abstract The impact of increased greenhouse gases (GHG) and aerosols concentrations upon the West African monsoon (WAM) is investigated for the late twenty-first century period using the Météo-France ARPEGE-IFS high-resolution atmospheric model. Perturbed (2070–2100) and current (1961–2000) climates are compared using the model in time-slice mode. The model is forced by global sea surface temperatures provided by two transient scenarios performed with low-resolution coupled models and by two GHG evolution scenarios, SRES-A2 and SRES-B2. Comparing to reanalysis and observed data sets, the model is able to reproduce a realistic seasonal cycle of WAM despite a clear underestimation of the African Easterly Jet (AEJ) during the boreal summer. Mean temperature change indicates a global warming over the continent (stronger over North and South Africa). Simulated precipitation change at the end of the twenty-first century shows an increase in precipitation over Sudan-Sahel linked to a strong positive feedback with surface evaporation. Along Guinea Gulf coast, rainfall regimes are driven by large-scale moisture advection. Moreover, results show a mean precipitation decrease (increase) in the most (less) enhanced GHG atmosphere over this region. Modification of the seasonal hydrological cycle consists in a rain increase during the monsoon onset. There is a significant increase in rainfall variance over the Sahel, which extends over the Guinea coast region in the moderate emission scenario. Enhanced precipitation over Sahel is linked to large-scale circulation changes, namely a weakening of the AEJ and an intensification of the Tropical Easterly Jet.

C. Caminade (✉) · L. Terray · E. Maisonnave
CERFACS, 42 Avenue G. Coriolis,
31057 Toulouse-Cedex, France
E-mail: caminade@cerfacs.fr
Tel.: +33-561-193040
E-mail: terray@cerfacs.fr
E-mail: Eric.Maisonnave@cerfacs.fr

1 Introduction

Since the pre-industrial period, greenhouse gases (GHG) concentration has exponentially increased. In particular, carbon dioxide (CO_2) concentration has increased in the atmosphere from 280 ppmv at the beginning of the industrialisation (since 1850) to 367 ppmv at the end of the twenty-first century (IPCC 2001). Emissions from fossil fuel combustion, deforestation are responsible for the observed GHG emission enhancement, resulting in an increase of the heat energy amount at the surface and thus by stronger values of global observed surface temperatures (Folland et al. 1992; Santer et al. 1996). According to demography and human activities projection on the next century, global warming will continue increasing with substantial consequences on climate (IPCC 2001).

Climate over West Africa is dominated by the Monsoon system. This seasonal reversal of the wind flow (linked to the temperature difference between sea surface and continent) brings moisture inland from the tropical Atlantic Ocean, and is responsible for the major part of precipitation during the boreal summer (July-August-September or JAS) over Sahel and Sudan. The agrarian activities and increasing local population strongly depend on the rainy season return. For instance, the persistent drought observed during the last few decades had dramatic agrarian and social consequences. Several studies have been performed to determine the climate processes that could potentially explain this decadal precipitation deficit. Several analyses highlight the links existing between various sea surface temperature (SST) patterns and precipitation variability over West Africa (Palmer 1986; Folland et al. 1986; Janicot and Fontaine 1996). At interannual time scale, Palmer (1986) suggests a major influence of El Niño Southern oscillation (ENSO) signature on precipitation over Sahel. Rowell (2001) explains in detail the teleconnection mechanism between the Tropical Pacific and West Africa. During warm ENSO events (El Niño), the interaction of atmo-

spheric equatorial Kelvin wave from the Tropical Pacific with an off-equator Rossby wave (response to the zonal SST gradient between the East Indian Ocean and West Pacific) reinforces large-scale subsidence over Africa. It induces weaker convective activity (direct effect) and reduces monsoon flow (indirect effect) over West Africa. At decadal time scale, Lamb (1978a, b) and Hastenrath (1984, 1990) highlight the influence of the so-called tropical Atlantic SST dipole on precipitation variability over Sahel. An impact of Indian Ocean SST anomalies on the multi-decadal trend contrasting wet and dry years over West Africa is also suggested by Shinoda and Kawamura (1994) and more recently by Bader and Latif (2003) and Giannini et al. (2003). At seasonal time scale, West African climate is very sensitive to the continental surface boundary conditions (Charney and Shukla 1981). Zheng and Eltahir (1998) document the impact of vegetation distribution on West Africa monsoon (WAM) system. They detail the impact of Guinea coast deforestation on surface net radiation and boundary layer entropy reduction, leading to weaker convection over the Sahel. Modelling studies using paleoclimatic time-scale experiments suggest the possible expansion of vegetation cover of the Saharan land area under increased CO_2 concentrations forcing which trigger increased rainfall over West Africa through vegetation-atmosphere feedbacks (Claussen et al. 2002; Brovkin 2002). Albedo and surface roughness also play an important role (Laval and Picon 1986) on WAM. An enhancement of surface albedo is associated with a stronger Tropical Easterly Jet (TEJ) and weaker easterlies at low altitude, and thus lower precipitation over West Africa.

Recent studies have been performed to highlight the impact of GHG emission scenarios on WAM (Hulme 1994; Maynard et al. 2002; Johns et al. 2003). The results agree on a significant warming over West Africa for the end of the twenty-first century. However, the results about the hydrological cycle modification are not as consistent. Maynard et al. (2002) show an enhancement of precipitation over West and North Africa [according to the Special Report on Emission Scenario (SRES-B2) from the Intergovernmental Panel on Climate Change (IPCC)]. Hulme (1994) suggests a rainfall deficit over the northern sector of the continent (IPCC SRES-A2 emissions projections). In these studies, the numerical experiments used classical low-resolution CGCM (coupled general circulation models), and did not consider uncertainty sources due to the selected GHG emission scenario and the internal climate variability. Paeth et al. (2003) study distinguishes SST versus anthropogenic climate change signals upon West African rainfall. Their model (only forced by observed SST) was able to reproduce the observed drought tendency following the 1960s over the Sahelian area. The most interesting feature of this work is that the additional effect of GHG forcing in the model induces significantly positive rainfall anomalies in recent years, as observed since the 1990s above West Africa. This result is consistent with their climate change scenario simulations predicting an intensification of the hydrological cycle over the Guinea coast and Sahel region. They suggest that the underlying physical mechanism linking the radiative forcing to the monsoonal rainfall enhancement works via warming of the tropical Atlantic Ocean.

Although numerical experiments performed using CGCMs are the most common tools to study future climate changes, the traditional coarse grid resolution is such that it does not capture the complex regional precipitation and temperature patterns over the African continent. In addition, climate change information in terms of impacts is required at finer spatial scales than the classic GCM grid one. One solution to obtain enhanced regional information is to use higher resolution atmosphere stand alone GCMs to simulate specific periods of interest (“time-slices”) using oceanic boundary forcing from coupled GCM transient scenario simulations (Cubasch et al. 1995). This approach allows circumventing the expensive cost of running the century-long coupled simulations. In this study, two time slices have been selected namely 1961–2000 (present climate) and 2070–2100 (perturbed climate).

The purpose of this work is first to determine the impact of different greenhouse gases and sulphate emission scenarios on the West African climate, and then to highlight the physical processes responsible of the WAM system modification using the ARPEGE-IFS variable resolution model in time-slice mode. In addition this work is a first attempt to estimate the relative uncertainties of WAM changes due to both SST boundaries forcing (coming from low-resolution CGCM transient scenario simulations) and selected emission scenarios. Furthermore, West African precipitation variability modification is investigated in the scenarios experiments.

In Sect. 2, the model, the numerical experiments and the observation data set will be described. A validation of the simulated climate for the current period over West Africa will be done in Sect. 3. Section 4 first investigates the impact of different GHG emission scenarios on WAM system, and highlights the hydrological cycle modification and the associated atmospheric dynamics change. Then, West African precipitation interannual variability change is detailed. Results will be summarized in Sect. 5, and future perspectives will be given.

2 Model and numerical experiments description

2.1 Model details

The Météo-France ARPEGE-IFS variable resolution version used in this study is described in detail in Gibelin and Déqué (2003). The model uses a semi-lagrangian advection scheme, a two time level discretization and a 30 min step. The spectral truncation is T106 and hybrid coordinates (Simmons and Burridge 1981) are used for the vertical discretization with 31 vertical levels. The

radiative forcing, including the effect of 4 GHG (CO_2, CH_4, N_2O and CFC) in addition to water vapour and ozone and of five aerosol types (land, sea, urban, desert and sulphates), is calculated by the Morcrette scheme (Morcrette 1990).

The stretched grid has the pole located in the Mediterranean Sea (40°N, 12°E) with a stretching factor of 3. The most refined horizontal resolution is 0.5×0.5° while the coarse grid covers most of the Pacific with a resolution close to 3.75×3.75°. Note that the resolution is relatively high over West and North Africa (1×1°). The ISBA (Douville et al. 2000) soil vegetation scheme is included. A four layers heat diffusion scheme is used, and the soil hydrology representation holds four reservoirs: canopy interception, snow, shallow surface and root layer reservoirs.

2.2 Experimental design

For the present climate (1961–2000), an ensemble of three simulations has been performed. The model is forced by monthly-observed SST from Reynolds data set (Smith et al. 1996) and by observed GHG concentration evolution, each simulation differing by its initial atmospheric condition. The ensemble mean for the present period will be referred to as CTRL in the following.

For future climate (2070–2099) two GHG emission scenarios (A2 and B2) are examined, estimated from different demographic, social and economic evolution factors as given by IPCC. Low resolution coupled simulations forced by the SRES-A2 and SRES-B2 GHG emission scenarios have been first performed with two CGCMs, respectively, HadCM3 and OPA-ARPEGE. For more details about the transient simulations, the reader is invited to refer to Johns et al. (2003) for HadCM3 and Royer et al. (2002) for OPA-ARPEGE. Then, monthly SST fields are created by superimposing the observed interannual variability (Reynolds data set) over the last 30 years on the mean change of global SST coming from the coupled model simulations over the 2070–2100 period. Finally, the variable resolution ARPEGE model is forced by these monthly SST fields and by the two GHG emission scenarios. Similarly to the present climate experimental set-up an ensemble of three simulations is performed for each configuration (SRES-A2 with boundary oceanic forcing coming from HadCM3, SRES-B2 with SST forcing provided by OPA-ARPEGE). The ensemble mean of these simulations will be referenced hereafter in the text as HCA2 (MFB2). These two configurations have been selected to contrast a strong forcing case (A2 and SST from HadCM3) versus a weak one (B2 and SST from OPA-ARPEGE).

Differences in the SST forcing fields come from different scenario and different physical parameterizations. In the following, the SST field forcing provided by a coupled model M (HC for HadCM3, MF for OPA-ARPEGE) with a GHG emission scenario G (A2 or B2) will be referenced as SST (M, G). The mean SST (HC, A2) change pattern exhibits a strong warming over Tropical Atlantic Ocean whereas SST (MF, B2) pattern reveals a quite uniform warming over this basin during boreal summer. Cross-atmospheric experiments (with SST (HC, B2) and SRES-B2 GHG emission scenario, and SST (MF, A2) with SRES-A2 scenario) have been performed to determine the relative impact of different SST and GHG emission scenarios forcing impact on WAM system. These atmospheric experiments will be respectively referenced in the text as MFA2 and HCB2. The entire experimental set-up is summarized in Table 1.

2.3 Observation data set

In order to assess the performance of the model in reproducing the present climate several observation data sets are examined.

Simulated precipitation and land surface temperature over Africa are compared to the global 0.5×0.5° resolution CRU (Climatic Research Unit) data set for the period 1961–1997 (http://www.cru.uea.ac.uk/~timm/grid/CRU_TS_2_0.html, Mitchell et al. submitted).

Pressure and dynamic fields will be compared to the NCEP-NCAR (National Centre of environmental prediction) monthly reanalysis data set over the 1961–1997 period. (http://www.cdc.noaa.gov/cdc/data.ncep.reanalysis.html#pressure for more explanation, Kalnay et al. 1996)

3 Model validation

In this section, the model ability to reproduce the observed climate over the present period will be considered through a comparison between one numerical experiment (DA9, Table 1) characterising one possible realisation of the climatic system and the NCEP-NCAR reanalysis and CRU data sets.

3.1 Monsoon dynamic (U, V, P)

The observed mean pressure pattern during JAS (Fig. 1a) depicts well-known large-scale structures: the Azores (over North Atlantic Ocean) and Ste Helene (South Atlantic) highs and low-pressure areas over Sahara and Brazilian Nordeste. The model is able to reproduce the main pressure structures (Fig. 1b); nevertheless, a northeast shift and an underestimation of the eastward extension of the Azores anticyclone core, with stronger values of pressure over Ste Helene can be noticed.

At 925 hPa, the observed wind field (Fig. 1a) during JAS exhibits the establishment of the monsoon regime over West Africa. A strong southwesterly flow coming from the Tropical Atlantic enters the continent (Gulf of

Table 1 Experimental set-up description

Ensemble mean experiment	Experiment(s)	SST forcing	GHG emission scenario	Period
HCA2	3 (DE6-DE7-DE8)	HadCM3	SRES-A2	2070–2100
MFB2	3(DC9-DC2-DC7)	OPA-ARPEGE	SRES-B2	2070–2100
MFA2	1 (DE9)	OPA-ARPEGE	SRES-A2	2070–2100
HCB2	1 (DE5)	HadCM3	SRES-B2	2070–2100
CTRL	3 (DA9-DE3-DE4)	Reynolds data-set	Estimated over the last 40 years	1960–2000

Guinea) and a weaker dry northeasterly Harmattan flow comes from the Sahara. The model (Fig. 1b) underestimates the southwesterly monsoon flow entering West Africa. Note also that simulated wind field values are weaker over the continent (underestimation of the Harmattan flow). Moreover, the wind direction is well reproduced by the model over the continent and Gulf of Guinea. Nevertheless, the trade wind convergence area is distributed along 8°N in NCEP whereas the model depicts a tilted convergence zone. Simulated wind fields centred on the Azores anticyclone show a divergent circulation whereas observed values exhibit a more rotational configuration.

The TEJ (near 200 hPa) is a thermal wind linked to the temperature difference existing between high Tibetan plateau and the Indian Ocean. The main wind core is located over Indian Ocean and extends westward over the Sahel (Fig. 2a). The TEJ core is underestimated by the model (by 50%) and shifted to the southeast. Its westward extension over West Africa is weaker (underestimated by 60%) in the numerical experiments (Fig. 2b).

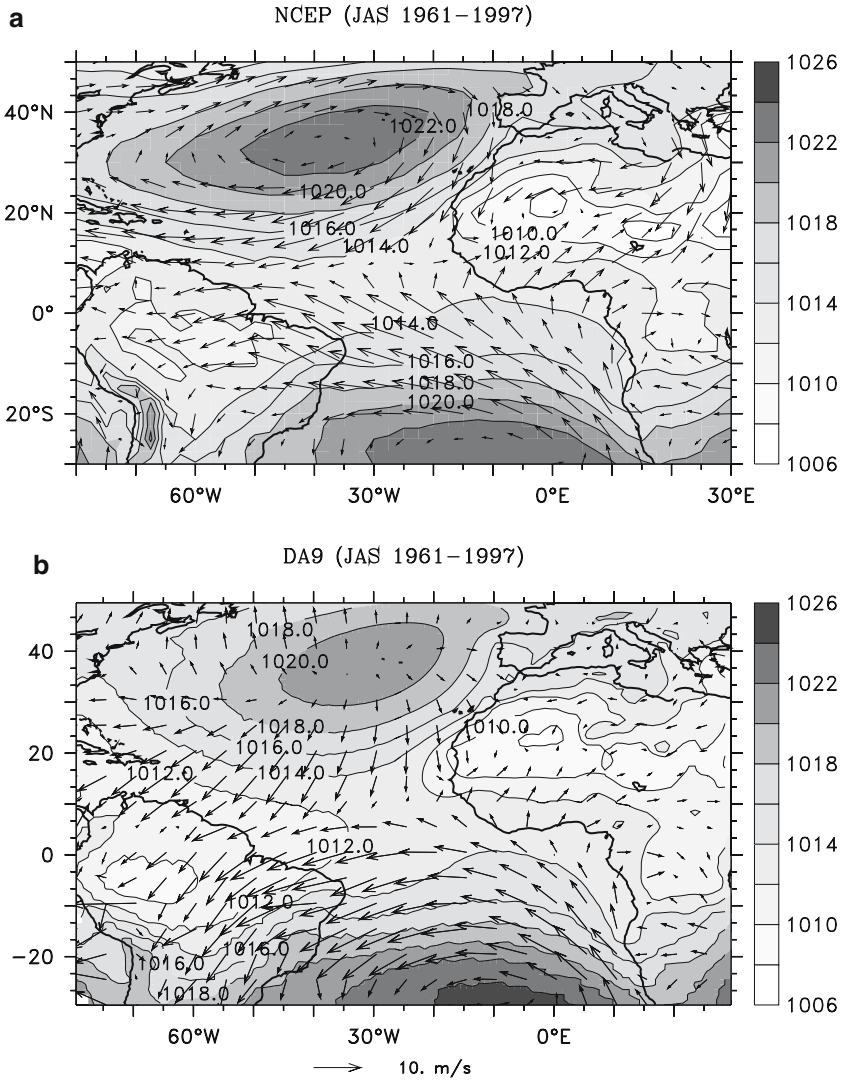

Fig. 1 Mean sea level pressure (*shading*) in hPa with superimposed mean wind vector field (m/s) at 925 hPa (JAS 1961–1997) for NCEP reanalysis (**a**) and DA9 (**b**)

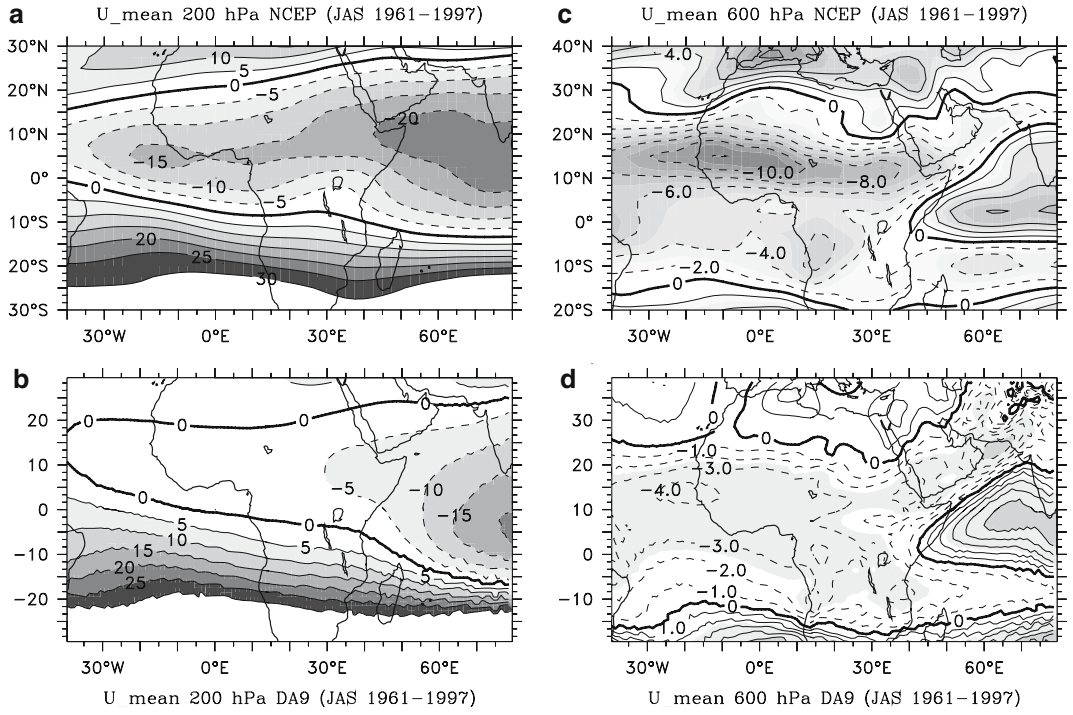

Fig. 2 Mean zonal wind (JAS 1961–1997) for observations from NCEP at **a** 200 hPa and **c** 600 hPa , and DA9 simulation at **b** 200 hPa and **d** 600 hPa

The African easterly jet (AEJ) is a moderate jet stream (centred on 15°N over the Sahelian area) caused by the thermal contrast existing between West Africa continent and the Tropical Atlantic ocean (Fig. 2c). It plays a dominant role in organizing the mesoscale convective systems and generating synoptic-scale African easterly waves. The northward seasonal migration of the AEJ core during boreal summer (Grist and Nicholson 2001) is well simulated (not shown). Nevertheless, the model underestimates the extension and the AEJ intensity core by 60% (Fig. 2d).

3.2 Precipitation and temperature

The observed precipitation pattern is distributed (Fig. 3a) on a wide latitude band from 5°S to 18°N [linked to the inter tropical convergence zone (ITCZ) position during JAS], and high precipitation areas are confined over Guinea coast (from Senegal to Liberia), Nigeria coast and Ethiopia (denoting a regional effect of high Ethiopian plateau on rainfall). The precipitation pattern is well reproduced in the present climate simulation (Fig. 3b) despite local differences (underestimation of strong precipitation areas along the Guinea coast and Niger).

The shape of the simulated ITCZ is comparable to observations but extends slightly too far to the North (this GCM bias has already been shown for other models by Moron 2003).

Maximum temperatures cover the entire Sahara and Maghreb while minima are observed over South Africa (Fig. 4a). Simulated temperature pattern (Fig. 4b) agrees reasonably with observations despite a small cold bias over West Africa.

In conclusion, results show that the ARPEGE-IFS model is able to capture the main features of the WAM system during JAS, in spite of the significant bias concerning the AEJ representation.

4 Impact of different greenhouse gases emission scenarios on WAM system

The purpose of this part is to document the modification of the simulated WAM system in response to different scenarios for greenhouse gases and sulfate emissions at the end of the twenty-first century.

4.1 Mean temperature changes

The distribution of surface air temperature difference in JAS between the control (CTRL) and the two scenarios experiments (HCA2, MFB2) is shown in Fig. 5. Globally, warming is stronger over continent than over sea (not shown) due to the strong thermal inertia of the oceans, and by a quick response of land temperatures to higher longwave radiation forcing in an enhanced GHG atmosphere. These patterns exhibit a global enhancement of temperature over Africa, with maxima located over Maghreb, Egypt and South Africa region. The temperature increase is weaker over Sahel–Sudan, in agreement with the modification of long-wave surface heat flux

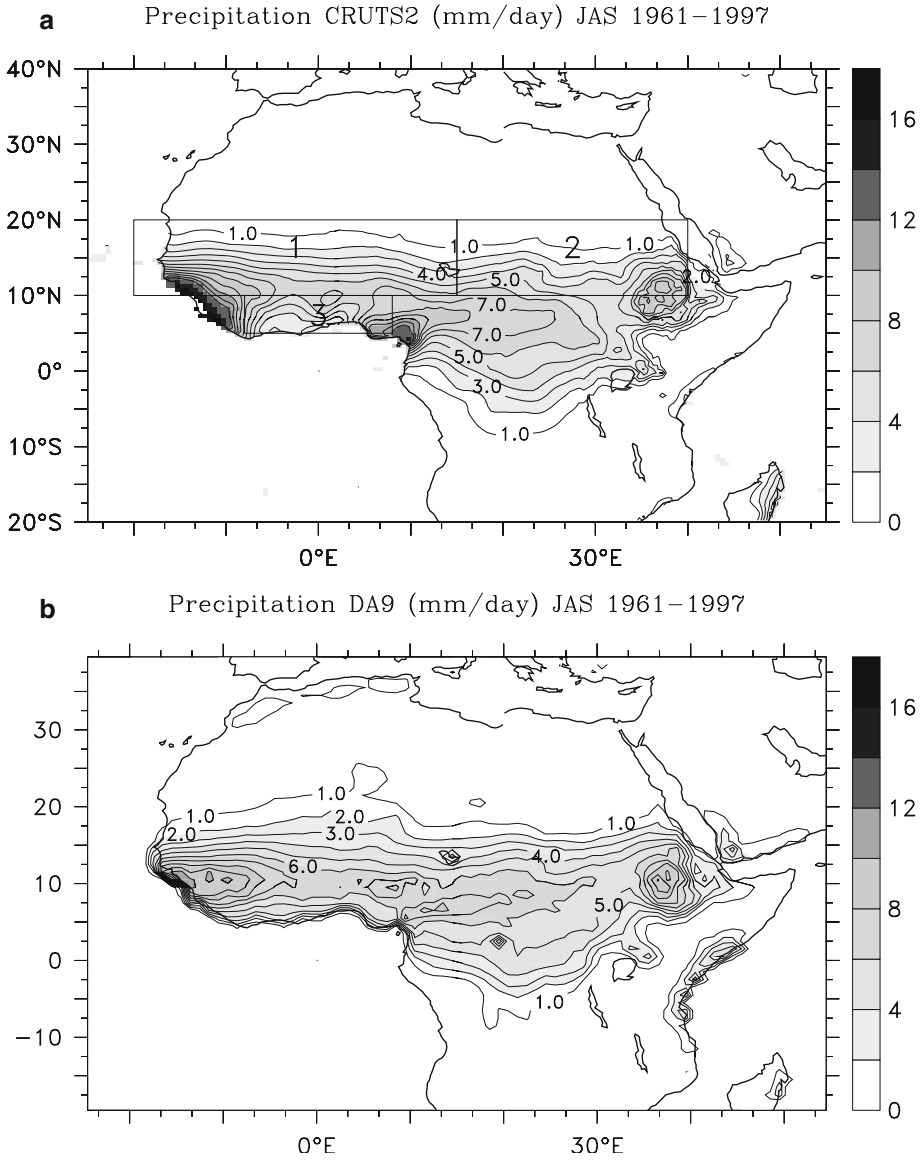

Fig. 3 Average precipitation (mm/day) in JAS (1961–1997) from **a** observation from the CRUTS2 data set and **b** DA9 numerical experiment. Grid box 1 defines the Sahelian area (10°N–20°N, 20°W–15°E), box 2 the Sudan region (10°N–20°N, 15°E–40°E), and grid box 3 delimits the Guinea coast area (5°N–10°N, 8°W–8°E)

spatial distribution (not shown). Note that the temperature change signal is sufficiently strong all over the African continent to be significant at the 99% level as estimated by a *t* test (not shown). Contrasting HCA2 (Fig. 5a) and MFB2 (Fig. 5b) minus CTRL African surface temperatures patterns, stronger values can be seen in the most enhanced GHG atmosphere excepted over South Africa area and Egypt where there's no striking regional differences. Temperatures predicted by HCA2 experiment are warmer than those simulated by MFB2 over Sudan and Sahel (by ≈1°C) during the boreal summer.

4.2 Hydrological cycle

4.2.1 Mean changes

Whatever the GHG emission scenario and the SST forcing, the mean precipitation difference over Africa during JAS (Fig. 6, left column) shows a global enhancement of the hydrological cycle over Sahel and Sudan. Significant weaker precipitation is observed over Cameroon, Congo and Gabon. This result is consistent with studies done by Maynard et al (2002). The simulated rainfall increase over the Sahelian region (≈0.4 mm/day) is the same in the two experiments. Precipitation change patterns over Gulf of Guinea region seem to be significantly different depending on the selected emission scenario and SST forcing. Reduced precipitation is depicted over Guinea coast (Fig. 6a) in HCA2, whereas according to MFB2 (Fig. 6b) there is no significant precipitation difference. Rainfall enhancement over Sudan is slightly stronger in MFB2 numerical experiment by 0.2 mm/day. The HCA2 precipitation pattern might be interpreted as a northward shift of the ITCZ as characterised by the mean change in outgoing long-wave radiation (OLR, not shown).

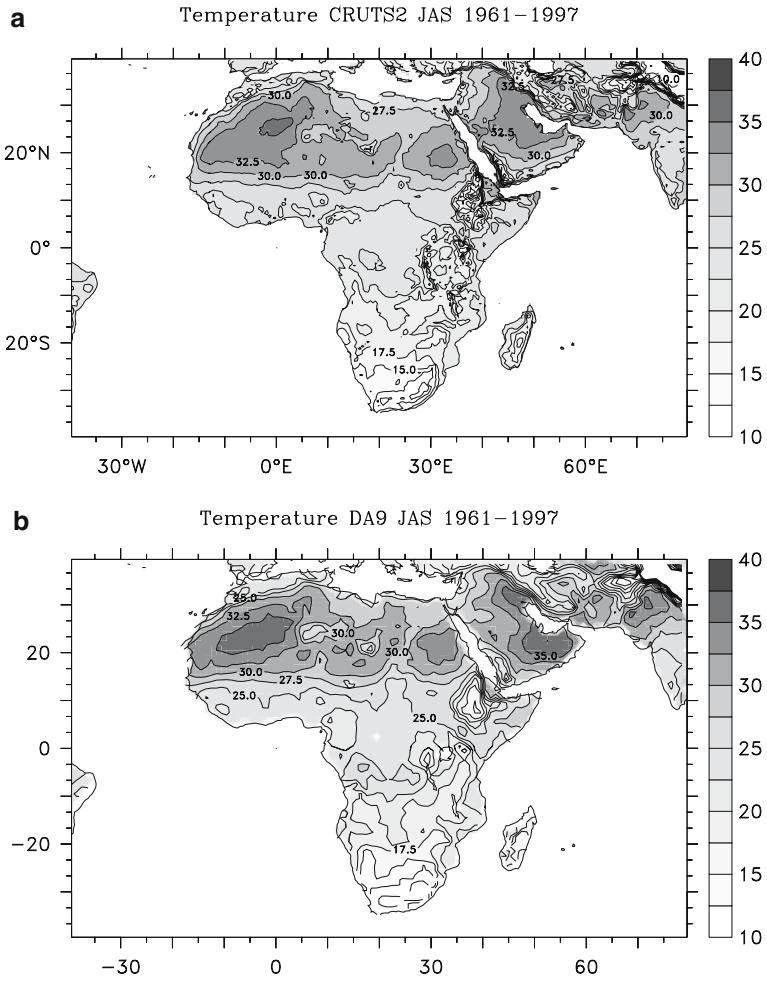

Fig. 4 Mean land surface temperature (°C) in JAS (1961–1997) from **a** observation (CRUTS2) and **b** DA9 experiment

4.2.2 Precipitation seasonal cycle

Figure 7 shows the mean precipitation seasonal cycle over three regions of interest: the Sahel (Fig. 3a, box 1), Sudan (box 2) and the Gulf of Guinea (box 3). Over Sudan and Sahel, observed maximum precipitation occurs during JAS, with a peak structure corresponding to the most northward position reached by the ITCZ during its migration. The observed mean seasonal cycle of precipitation over Guinea shows two maxima occurring during June and September with a flat profile during the establishment of the monsoon regime (JAS). The fast rainfall increase (March–June) corresponds to the northward migration of the ITCZ and the second peak (September–October) is linked to its retreat.

The seasonal cycle of simulated precipitation agrees with observations over Sahel, Sudan and Guinea. Nevertheless, there is a slight overestimation of rainfall during the pre-onset (May–June) and the collapse (October–November) of the African monsoon whatever the location. Note also that precipitation is overestimated (by 0.5 mm/day) over the Sudan.

Different precipitation regimes have been previously highlighted: increase of precipitation over Sahel and Sudan (more marked with MFB2), and a rainfall deficit (no significant difference) over the Gulf of Guinea in HCA2 (MFB2). Whatever scenario and SST forcing considered, a slight intensification of the seasonal hydrological cycle during the onset (May–June) and the establishment (JAS) of the West African monsoon regime is obtained over Sahel and Sudan. The simulated rainfall enhancement over Sahel is similar in the two scenario experiments. Note also that the rainfall increase concerning the Sudan region is stronger in MFB2 during July–August. Over the Guinean area, an increase of precipitation is shown during the onset (first peak during May–June) of the monsoon (more intense according HCA2). During JAS and the collapse (Second peak, September–October) of the monsoon regime, there is no significant change according to the MFB2 experiment whereas HCA2 mean seasonal hydrological cycle simulates a slight rainfall decrease over Guinea (consistent with Fig. 6a).

4.2.3 Physical process associated

Atmospheric water vapour has a short life-cycle, about 10 days stored in the atmospheric column. Furthermore

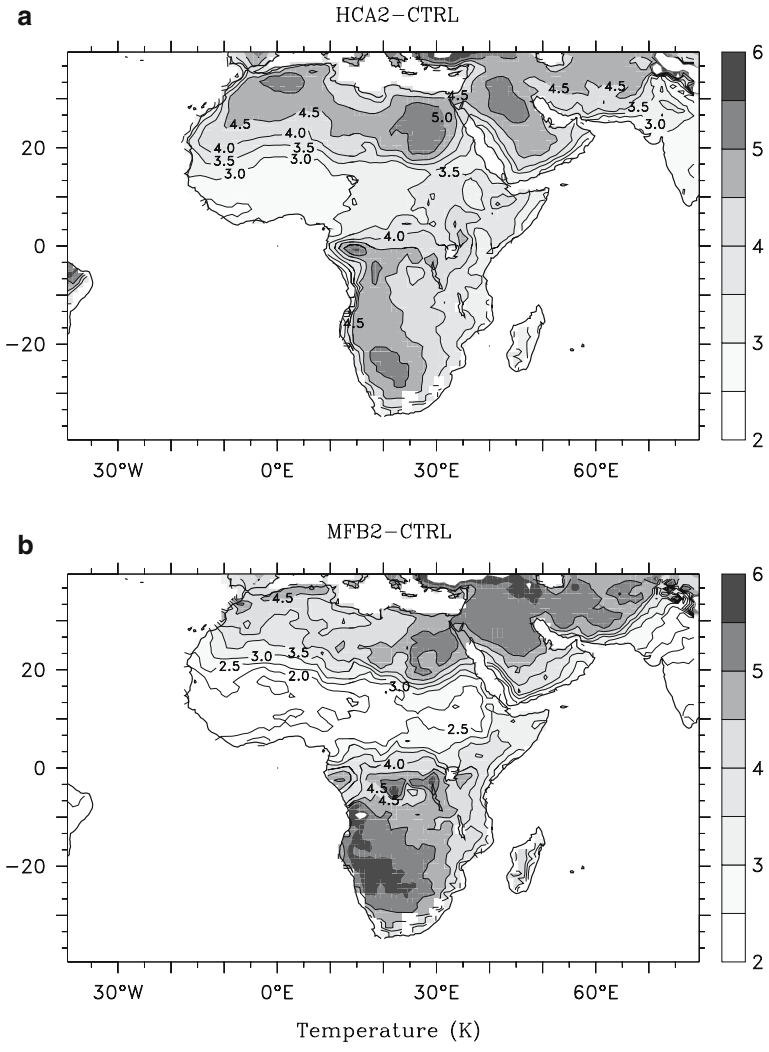

Fig. 5 Mean land surface temperature (K) changes, **a** HCA2-CTRL, **b** MFB2 -CTRL during boreal summer (JAS)

water vapour content budget is balanced at global scale. Thus, considering the time-scale we focus on (seasonal mean), to characterise the process responsible for precipitation change in the experiments, it will be considered that the small variations of atmospheric water content are negligible. Thus, the difference between precipitation (P) and evaporation (E) being equal to the atmospheric water content at a given instant, is balanced by atmospheric moisture convergence. Contrasting E anomalies patterns (Fig. 6c, d) between the two experiments, results show an enhancement of surface evaporation over Sudan and Sahel in agreement with an increase of precipitation over this area (positive feedback). The evaporation increase is greater over Sudan than over Sahelian region. Nevertheless, the enhancement of surface evaporation over Sudan-Sahel is weaker in HCA2 (Fig. 6c) compared to MFB2 (with a similar pattern, Fig. 6d). A weakening of surface evaporation is simulated over Cameroon, Congo and Gabon (more marked in HCA2–CTRL).

Figure 8 shows the anomalous vertically integrated moisture convergence (P–E) with superimposed low-level (integrated between 1000 and 850 hPa) specific humidity advection characterizing the monsoon flow over West Africa. Important differences between HCA2 and MFB2 experiments can be seen along the Gulf of Guinea and Sahel.

In HCA2 (Fig. 8a), strong significant values of moisture divergence are depicted along the Guinea coast with weaker monsoon flow entering the continent, and no significant differences over Sahel and Sudan. This pattern corresponds to a northward shift of the ITCZ and is consistent with the precipitation pattern (Fig. 6a).

Despite the weakening of the monsoon flow coming from Guinea gulf, low-level humidity transport coming from Tropical Atlantic Ocean is stronger over the sahelian area.

The mean changes in MFB2 (Fig. 8b) show quasi-opposite results above the Gulf of Guinea: stronger low-level monsoon flow entering the continent with a strong enhancement of vertically integrated moisture convergence.

Over Sudan, the enhanced monsoon rainfall is associated with a strong increase in surface evaporation. In

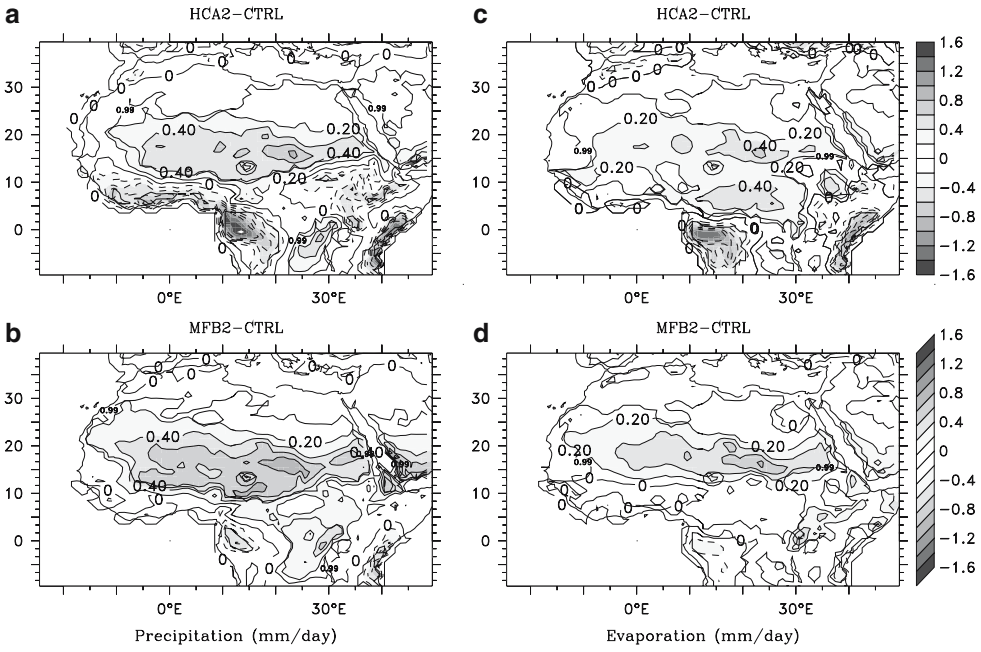

Fig. 6 *Left*: Precipitation anomalies (mm/day) between HCA2 (**a**), MFB2 (**b**) scenario prediction (2070–2100) and control experiments (CTRL) during JAS. *Right*: Idem for evaporation anomalies (mm/day), HCA2-CTRL (**c**), MFB2 –CTRL (**d**). *Bold line areas* denote response areas with the significance at the 99% level as estimated by a *t* test

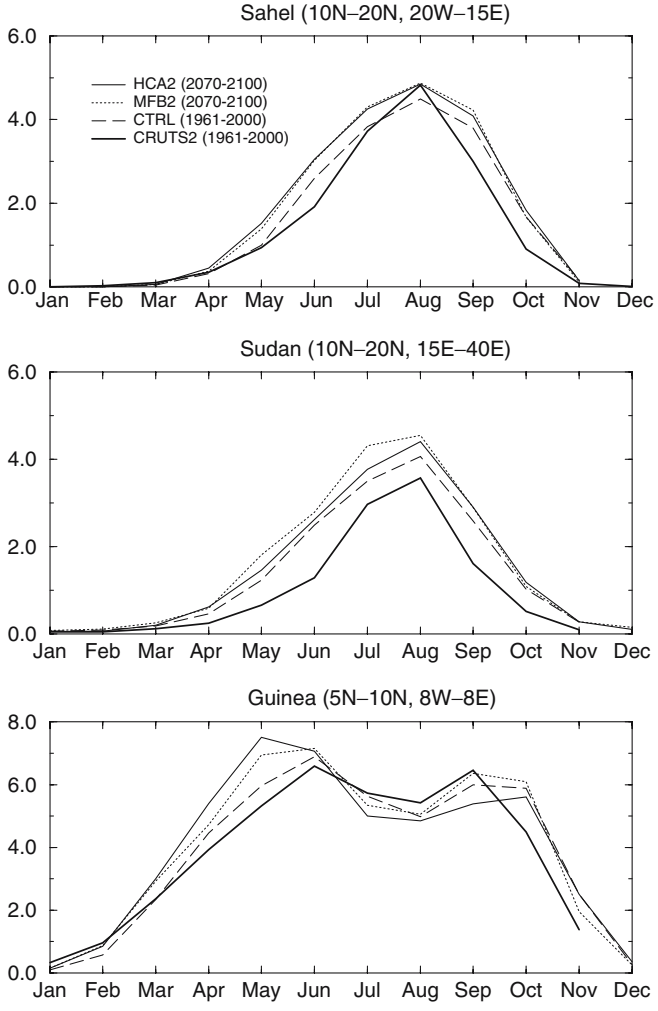

Fig. 7 Mean seasonal cycle of precipitation (mm/day) over Sahel, Sudan and Gulf of Guinea

perturbed climate (whatever the scenario experiment selected) the physical process responsible of the precipitation reinforcement above Sudan is a strong local positive feedback of evaporation, low-layer humidity advection playing a minor role. Above Sahel, the convective activity is more intense in an enhanced GHG atmosphere whatever the scenario considered. The summer monsoon rainfall is enhanced due to an increase of moisture advected from Tropical Atlantic Ocean and also to enhanced surface evaporation. Over Guinea coast, the precipitation increase (decrease) is primary linked to an increase of moisture advected by the large-scale flow, local evaporation anomalies being negligible. The climatic precipitation signal is very different (weaker/stronger monsoon flow) between the two experiments selected here above the Guinean area. These results are in agreement with studies of Lamb (1983). Gong and Eltahir (1996) who characterized evaporation over Tropical Atlantic as a primary moisture source for West Africa Monsoon. Considering HCA2 wind pattern, a meridian dipole structure of the 600 hPa zonal wind exhibits an increase over Equatorial Guinea with a decrease over the South Atlantic basin along the African coast (Fig. 9a). A strong increase of the zonal wind at 200 hPa over South Africa and a decrease over the South Indian basin can be noticed too (Fig. 9c). In MFB2 experiment, a weakening of the south part of the AEJ core with a northward extension (Fig. 9b) has been characterized. A westward extension of the TEJ (Fig. 9d) and its reinforcement can be noticed too. This change (weakening of the AEJ and intensification of the TEJ) has been linked to the precipitation increase over Sahel in previous studies (Kidson et al. 1977). MFB2 patterns are in agreement with studies done by Maynard et al. (2002) who characterised a more vigorous hydro-

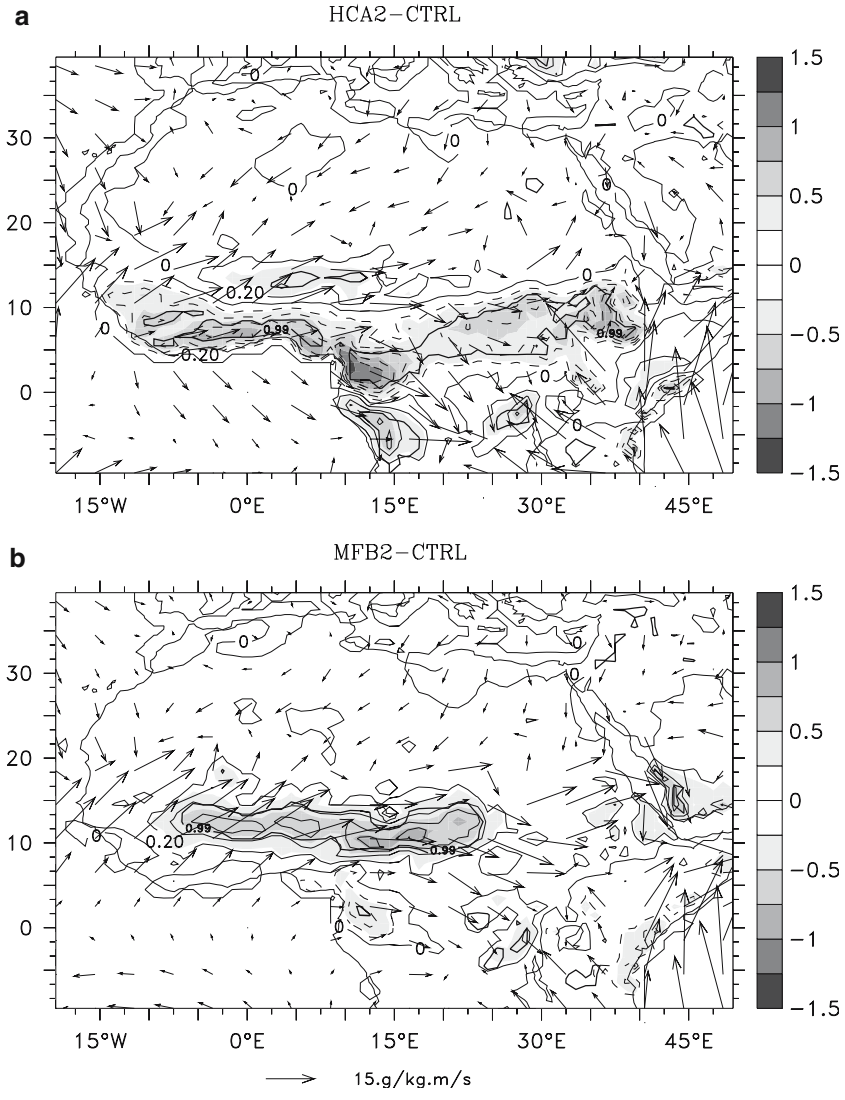

Fig. 8 Vertically integrated moisture convergence anomalies (P–E) in mm/day (*shading*) for JAS with superimposed low layer (integrated between 925 and 850 hPa) relative humidity advection in g/kg m/s (vector field). HCA2-CTRL (**a**), MFB2-CTRL (**b**). *Bold line areas* denote response areas with the significance at the 99% level as estimated by a *t* test

logical cycle, an enhancement of the monsoon flow, a weakening of the AEJ and an intensification of Southern Hemisphere Hadley cell using low resolution coupled experiments with SRES-B2 GHG emission scenario. The mean dynamic change in HCA2 cannot be linked to precipitation change over West Africa.

As a summary, whatever experiment selected, an increase of local surface evaporation, related to the surface warming is responsible of the summer rainfall increase over Sudan. The advected humidity flow coming from Tropical Atlantic Ocean is responsible of precipitation regime over the Gulf of Guinea. It is consistent with the fact that in HCA2 (MFB2) experiment, the weakening (strengthening) of the incoming monsoon flow is primary responsible of the rainfall deficit (excedent) over Guinea coast. Above Sahel, both surface evaporation feedback on precipitation and enhanced humidity transport are responsible of the simulated rainfall increase. MFB2 experiment is characterized by a weakening (strengthening) of the AEJ (TEJ) while no significant dynamical changes appear in HCA2.

4.2.4 Interannual variability changes

Recent studies based on paleoclimatic data show that interannual and decadal scale climate variability may experience change as a result of natural longer scale variability and anthropogenic greenhouse forcing. Considering the experimental setup of this study, attention will be given on the additional impact of the mean SST change (the observed interannual SST variability being superimposed in the future climate simulations) and the GHG emission scenario upon West African precipitation variability.

The present climate ensemble simulation (CTRL) is able to reasonably reproduce the observed rainfall interannual variability over Sahel but does not capture the multi-decadal trend contrasting wet (1960–1970) and dry (1970–2000) years over West Africa and especially over the Sahel region (not shown). Moreover, the time period being relatively short (30 years) in the GHG emission scenario experiments the main focus will be on interannual variability changes. The precipitation data is fil-

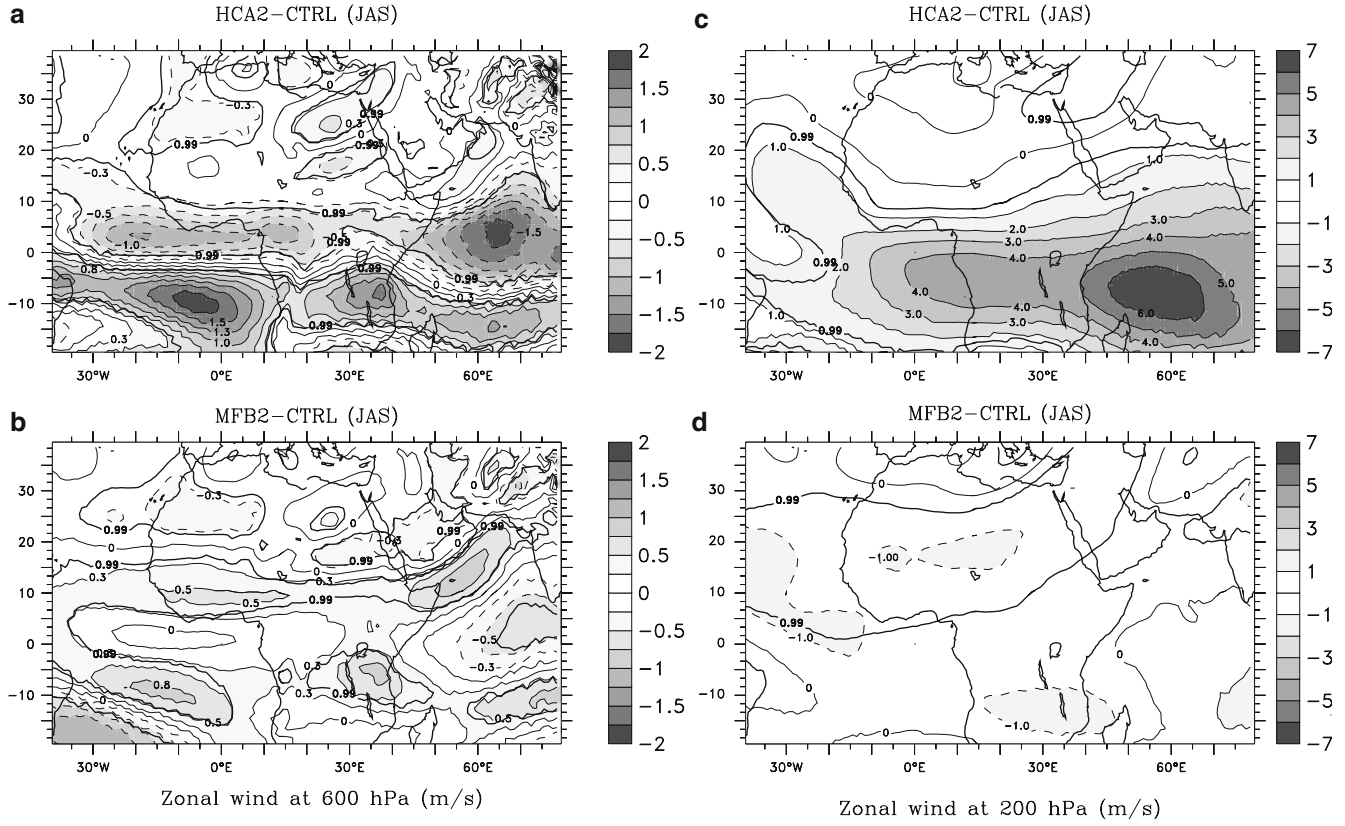

Fig. 9 Mean zonal wind difference (m/s) between HCA2 (*top*), MFB2 (*bottom*) and CTRL at 600 (left column) and 200 hPa (*right column*) during boreal summer (JAS). *Bold line areas* denote response areas with the significance at the 99% level as estimated by a *t* test

tered using a highpass filter (with a 8-year cut-off) in order to study variability changes. Relative variance difference is displayed between each scenario and the control ensemble on Fig. 10. Results show a significant variance increase between the scenario experiments and the control simulations over West Africa (Fig. 10a, b). Focusing on the (HC, A2) ensemble (Fig. 10a), a large variance increase (from 10 to 40%) is displayed over the sahelian area, whereas no significant differences can be seen over the Guinean coast region. Moreover maximum changes (30–50%) are localized between 10°N and 18°N. Considering the (MF, B2) ensemble (Fig. 10b), the variance increase is stronger than in the (HC, A2) ensemble and extends further south over the Guinean area (10–20%). Maximum changes (30–40%) are displayed over the band 5–15°N. A cross section of zonal mean variance summarizes all these results (Fig. 10c). Whereas the (MF, B2) variance distribution is clearly wider and increased over the whole West African domain compared to the control ensemble, that of (HC, A2) does not significantly differ from the present climate one over the Guinean region (5–10°N), and significantly increases over the Sahel.

A principal component analysis (PCA) to filtered summer precipitation (for each ensemble) over West Africa (0°N to 20°N, 16°W to 20°E) is used (Fig. 11) to analyse these variability changes. The analysis relies only upon the first precipitation mode because no significant changes are found for the second one between the control and the scenario experiments. The first precipitation mode exhibits positive rainfall anomalies along the Guinea coast in the control ensemble (Fig. 11a). This mode has been well documented in previous work (Giannini et al. 2003) and is clearly associated with warm SST anomalies in the southeastern tropical Atlantic Ocean. In (MF, B2) ensemble, the EOF spatial structure clearly extends northward with increased amplitude (Fig. 11b). Considering (HC, A2) the distribution of the first precipitation mode is clearly shifted northward, with centres of action corresponding to maximum variance changes (Figs. 10a, 11c). The first mode explained variance significantly increases in the scenario ensemble (~30%) compared to the control one (~20%).

While the (MF, B2) SST pattern shows a homogeneous warming over the Tropical Atlantic basin (Fig. 12b), (HC, A2) reveals an increase of the cross-equatorial SST gradient (Fig. 12a). Strong warm SST anomalies (~2.5°C) can be seen off Mauritanian coast, and weaker ones (~1.2°C) along the equatorial Atlantic cold tongue and Angola coast (Fig. 12a). Decadal variations of the Atlantic cross-equatorial SST gradient are

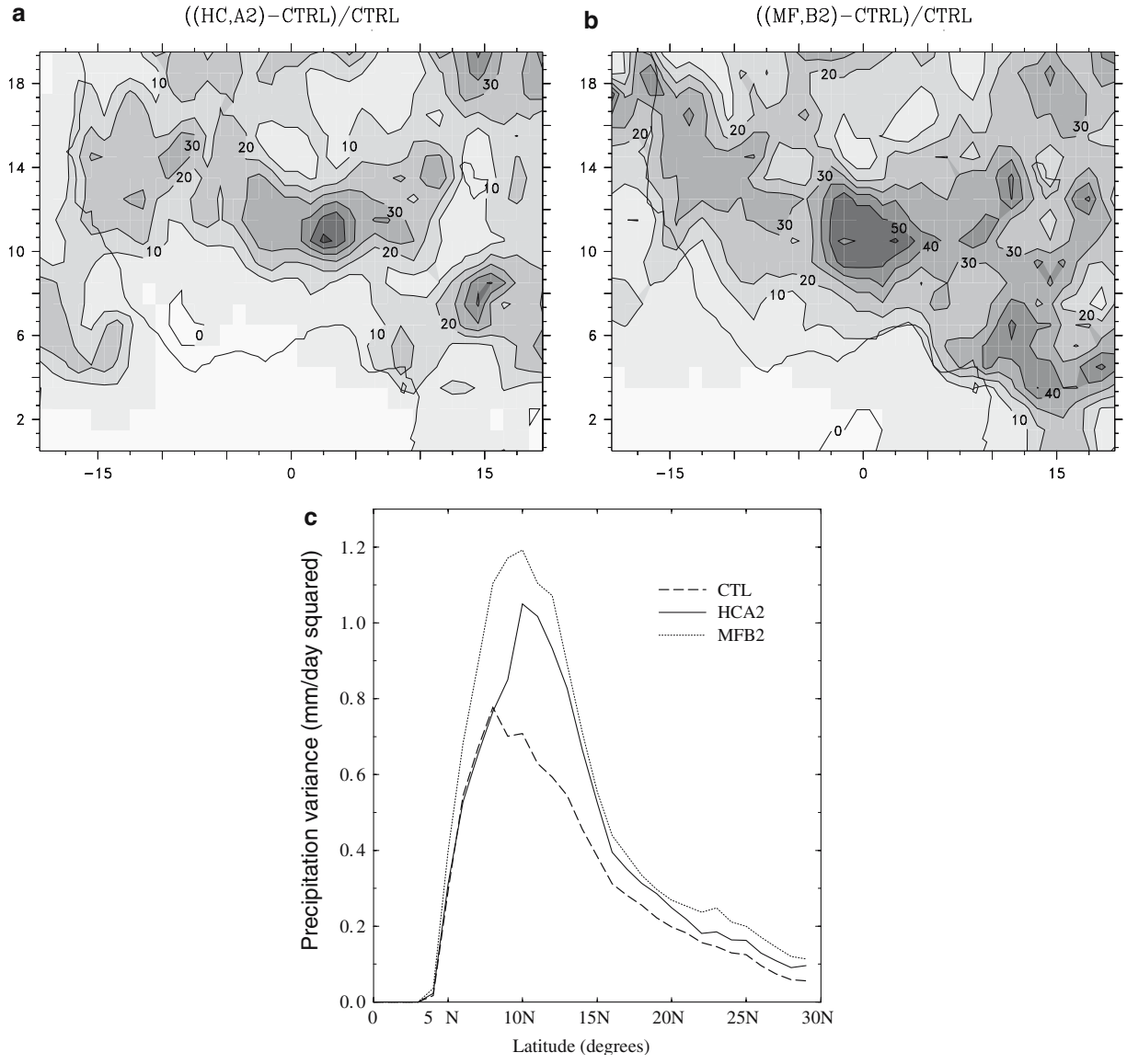

Fig. 10 *Upper panel*: Relative change in precipitation interannual variance (%) for (HC, A2) (Fig. 10a) and (MF, B2) (Fig. 10b). *Lower panel*: Zonal mean precipitation variance (mm/day squared) averaged between 15°W–10°E for each ensemble

linked to a meridional shift of the ITCZ and thus to precipitation regimes over Sahel and Guinea (Hastenrath 1990). This SST pattern is associated with a dipole contrasting positive (negative) rainfall anomalies over Sahel (Guinea). The impact of mean SST difference on West African precipitation variability could be interpreted as follows. The increase of the cross-equatorial Atlantic SST gradient shifts the mean position of the ITCZ northward, thus causing the rainfall variance to increase over Sahel in the A2 ensemble (as confirmed by EOF and variance analysis). Furthermore, there is a strengthening of the Atlantic SST forcing influence upon the rainfall interannual variability in the (HC, A2) scenario (not shown). Considering (MF, B2) ensemble, the increase of filtered rainfall variance is extended over the whole West African domain, while the mean SST warming is quite uniform over the Atlantic basin. An increase in the mean monsoon flow is depicted in (MF, B2) whereas enhanced divergence is shown over Guinea in (HC, A2) (Fig. 8). This dynamic configuration is consistent with an increase (no significant modification) of rainfall variability in B2 (A2) ensemble over the Guinean area.

Moreover, a normalized rainfall histogram has been performed for July to September monthly means, over the 2070–2099 period for each scenario ensemble and over 1960–1989 for the control one. The rainfall distribution over Sahel (Fig. 11d) is clearly shifted in (HC, A2) compared to the control ensemble. There is a significant increase of intense monthly precipitation and of the mean. (MF, B2) histogram over the sahelian area exhibits a wider structure than in the control ensemble. Rainfall mean and extremes are significantly increased. Whereas (HC, A2) distribution clearly exhibits a trans-

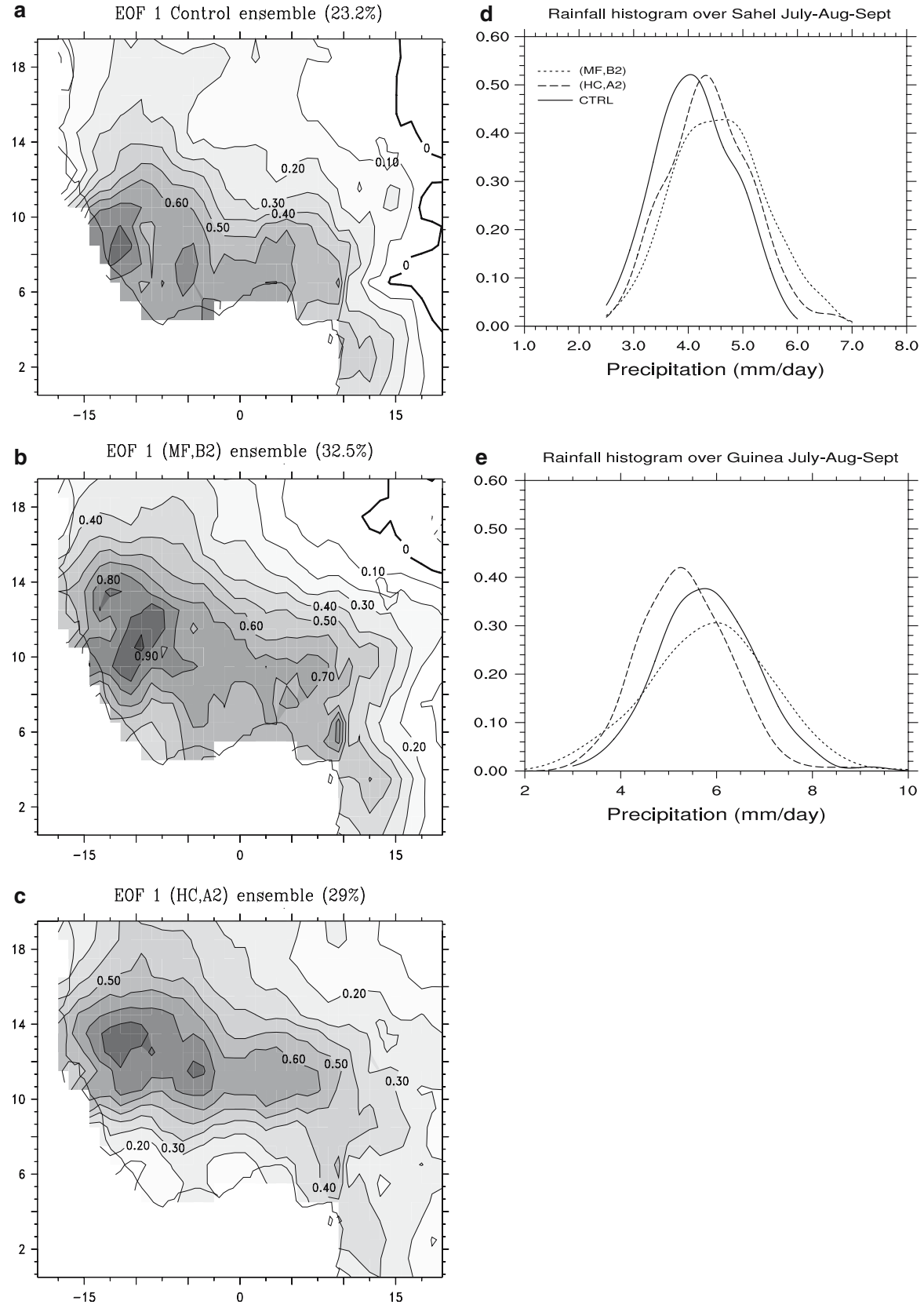

Fig. 11 First EOF mode of High-pass filtered precipitation (JAS) over West Africa. The first leading mode is displayed for the CTRL ensemble (**a**) over the 1960–1989 period, (MF, B2) (**b**) and (HC, A2) (**c**) ensemble over the 2070–2099 period. Normalized rainfall histogram computed from July to September montly means for each scenario simulations type over Sahel (**d**) and Guinea (**e**)

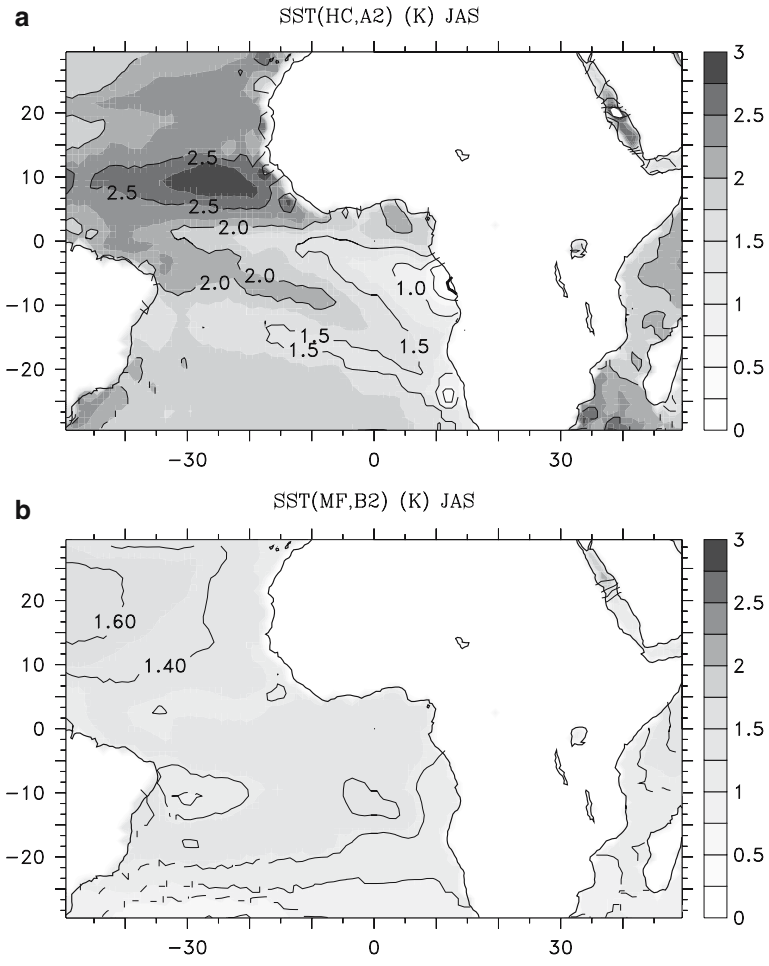

Fig. 12 Mean sea surface temperature changes (K) with respect to 1960–1989 observed SST for (HC, A2) (**a**) and (MF, B2) (**b**) during JAS

lation compared to the control ensemble, (MF, B2) distribution changes in the shape. Over Guinea (Fig. 11e) there is a decrease of the mean and intense rainfall in (HC, A2) and no clear modification of the histogram in (MF, B2) ensemble. All these results are consistent with mean precipitation changes for each scenario as described below in Sect. 4.2.1. Dealing with hydrological cycle variability modification relevant to climate change is not an easy task. Conceptual studies concerning global changes of rainfall extremes in an increased GHG atmosphere (Trenberth 1999) show that the surface warming caused by increased downwelling infrared radiation enhances both evaporation and the water-holding capacity of the atmosphere. As a consequence, the atmospheric moisture content increases, and thus, extreme events are favourized (all precipitation system feeding on the available moisture in the atmosphere). Considering the scenario experiments of this study, a significant increase of mean and "extremes" evaporation and atmospheric moisture content is revealed over West Africa (not shown). Moreover, the atmospheric moisture content and evaporation increase is stronger in the most enhanced GHG atmosphere (HC, A2). Over the sahelian region, all these results are consistent with Trenberth's conceptual study relating rainfall extremes increase and climate change. Nevertheless, a decrease of the mean and intense rainfall has been highlighted over the Guinean area, suggesting that other mechanisms influence regional scale changes.

4.2.5 Sensitivity analysis

To assess the atmospheric model sensitivity to different SST and GHG forcing, two additional experiments are considered. One simulation with the scenario B2 (A2) and SST fields provided by HadCM3 (OPA-ARPEGE) model has been performed and will be referenced as HCB2 (MFA2) (Table 1). Depending on which GHG emission scenario considered (A2 or B2), the hydrological cycle anomalies response of ARPEGE-IFS atmospheric model forced by the SSTs coming from HadCM3 (HC) coupled model exhibits the same pattern: a slight increase of precipitation over Sudan-Sahel and weaker precipitation over the Gulf of Guinea (Fig. 13a).

Weak significant precipitation differences can be shown over Senegal, Ethiopia and Guinea for MFA2 minus MFB2 pattern (Fig. 13b). Figure 13c, d shows the sensitivity of the model results to the choice of SST

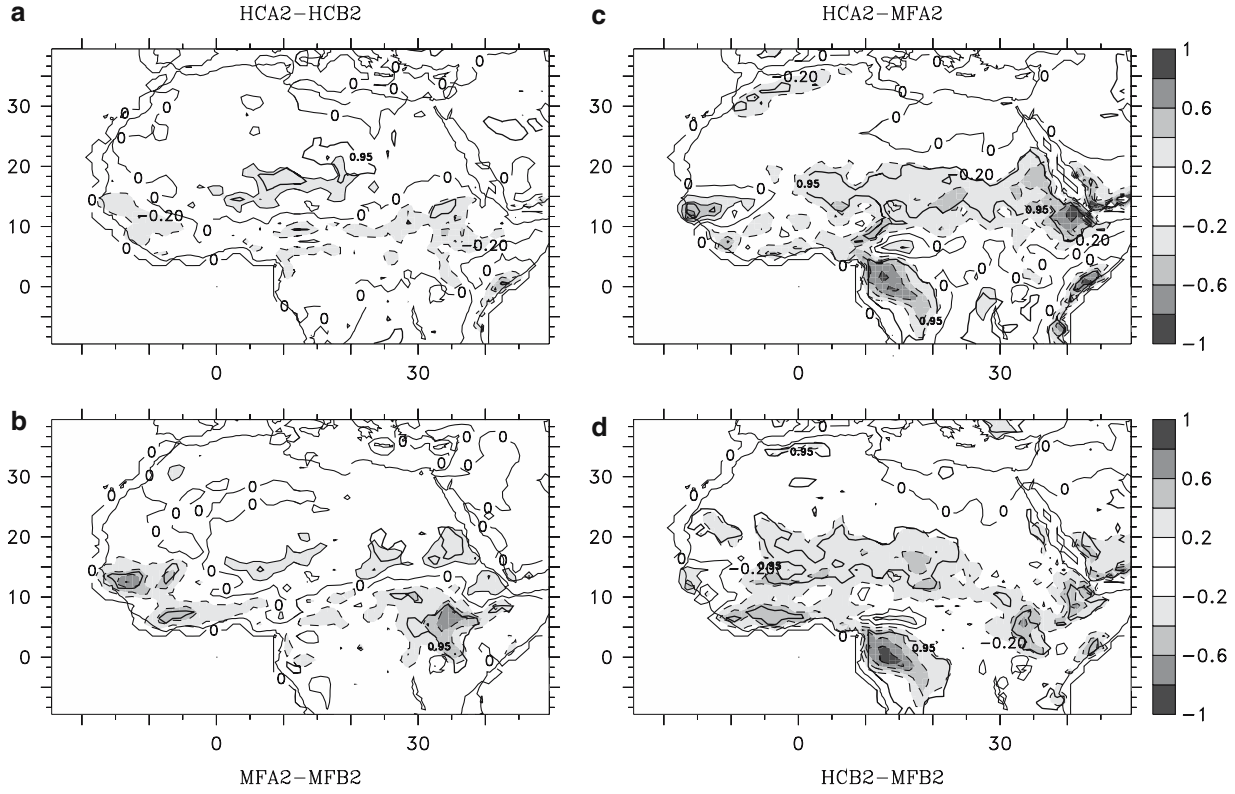

Fig. 13 Precipitations anomalies (mm/day) during JAS between the different cross-forced experiments. *Bold line areas* denote response areas with the significance at the 95% level as estimated by a *t* test

forcing for a given emission scenario. Over Sahel and Sudan, the impact of OPA-ARPEGE SST forcing on the summer rainfall increase is stronger (Fig. 13c). Over the Gulf of Guinea and Cameroon the precipitation decrease linked to HadCM3 SST forcing (Fig. 13d) is shown (northward shift of the ITCZ).

For a given coupled model, the mean SST change spatial pattern is similar despite the choice of the GHG emission scenario (A2 or B2, not shown). The only impact of the scenario is in term of magnitude (stronger temperatures in A2, weaker ones in B2). In this study, SST (HC, A2) (Fig. 12a) pattern is coherent with a northward shift of the ITCZ (see previous section). It leads to the precipitation increase over Sahel and the decrease of the hydrological cycle over Guinea. The increase of precipitation over Sudan-Sahel for MFA2 and MFB2 experiments can be primary linked to local process (evaporation enhancement), SST (MF, B2) warming being homogeneous over Atlantic basin.

To conclude, the simulated hydrological cycle sensitivity to SST forcing coming from the choice of the coupled model is stronger than the emission scenario selected. At multi-decadal time scales, previous work highlight large-scale SST pattern as the main factor that drives precipitation trend over West Africa (Giannini et al. 2003). The fact that climate variability over Africa or more generally within the latitude band is primary linked to SST patterns is coherent with these results.

5 Conclusion

The impact of anthropogenic emission scenario on WAM system is still controversial. If many studies agree on a global warming over Africa, there is not still a consensus about precipitation change and hydrological cycle modification, particularly at regional scale. In this study, changes in the African monsoon system at the end of the twenty-first century have been investigated using the ARPEGE-IFS variable resolution model, for two GHG emission evolution scenarios (SRES-A2 / SRES-B2) and two SST forcings. Results show a significant warming over the African continent, especially over Maghreb and South Africa, the temperature increase being stronger with SRES-A2 scenario.

Changes in precipitation associated with the global warming are characterized by an increase of rainfall over Sahel–Sudan (with a strong increase in surface evaporation), and a decrease (no significant differences) of precipitation along the Guinea Gulf considering HCA2 (MFB2) numerical experiments. Weaker monsoon flow (with strong moisture divergence) entering the continent, and a slight northward shift of the ITCZ has been highlighted with HCA2 experiment whereas MFB2 pattern depicts an enhancement of precipitation over Sahel with stronger monsoon flow (associated with

strong moisture convergence). The latter result is consistent with a weakening of the AEJ and a strengthening of the TEJ. West African precipitation variability changes in the scenario experiments have been highlighted. A significant increase of the rainfall variance over the Sahel is shown in the (HC, A2) ensemble (consistent with the mean increase of the Atlantic cross-equatorial SST gradient, and associated northward shift of the ITCZ). In (MF, B2), the precipitation variance increases over the whole West African domain. Impact of global warming on the seasonal cycle of precipitation is characterized by an increase of rain events during the onset of the West African monsoon. Note that precipitation intra-seasonal variability is not taking into account in this work. Sultan et al. (2003) have shown that rainfall and convection over West Africa are significantly modulated at two intra-seasonal time-scales, leading to variations of more than 30% of the seasonal signal.

Results show that uncertainties linked to the choice of the CGCM that provides the SST forcing are predominant compared to the direct impact of the emission scenario in this time-slice approach.

In this study, vegetation surface characteristics are fixed to the current period values over the period 2070–2100. Based on Zheng and Eltahir (1998) who show the importance of Guinea coast deforestation on precipitation regimes over West Africa, future studies must focus on this aspect, performing new experiments with full-coupled ocean–atmosphere–biosphere experiments. Numerical experiments have been carried out with the stretching pole centred in Mediterranean Sea. Although resolution is relatively high on the West African region to be confident in the results, it would be interesting to select the pole of stretching over the Guinean gulf centre at the equator. Recently, Maynard and Royer (2004) focus on the impact of land cover change on a greenhouse-warmed African climate. They use the same model version with the pole of stretching located above the Gulf of Guinea and consider SRES-B2 emission scenario. They show that realistic land cover change may have a small regional effect in projections of future climate (comparing to the impact of the scenario). It would be interesting to perform several other experiments with these configurations, considering A2 and B2 emission scenarios.

References

Bader J, Latif M (2003) The impact of decadal-scale Indian Ocean sea surface temperature anomalies on Sahelian rainfall and the North Atlantic Oscillation. Geol Res Lett 30(22):2169

Brovkin V (2002) Climate-vegetation interaction. J Physique IV:57–72

Charney JG, Shukla J (1981) Predictability of monsoons. In: Lighthill J, Pearce RP (eds) Monsoon dynamics. Cambridge University Press, Cambridge, pp 99–110

Claussen M, Brovkin V, Ganopolski A, Kubatzki C, Petoukhov V (2003) Climate Change in northern Africa: the past is not the future. Climatic Change 57(1–2):99–118

Cubasch U, Waszkewitz J, Hegerl G, Perlwitz J (1995) Regional climate changes as simulated in time-slice experiments. Climate Change 31:273–304

Douville H, Planton S, Royer JF, Stephenson DB, Tyteca S, Kergoat L, Lafont S, Betts RA (2000) The importance of vegetation feedbacks in doubled-CO_2 time slice experiments. J Geophys Res 105(14):841–861

Folland CK, TN Palmer, Parker DE (1986) Sahel rainfall and worldwide sea surface temperature 1901–1985. Nature 320:602–607

Folland CK, Karl T, Vinnikov KY (1992) Climate change 1992. In: Houghton JT, BA Callander, SK Varney (eds) The IPCC supplementary report. Cambridge University. Press, 200 pp

Giannini A, Saravanan R, Chang P (2003) Oceanic forcing of Sahel rainfall on interannual to interdecadal time scales. Science 302:1027–1030

Gibelin AL, Déqué M (2003) Anthropogenic climate change over the Mediterranean region simulated by a global variable resolution model. Clim Dynam 20:327–339

Gong C, Eltahir EAB (1996) Sources of moisture for rainfall in West Africa. Water Resour Res 32:3115–3121

Grist JP, Nicholson SE (2001) A study of the dynamics factors influencing the rainfall variability in the West African Sahel. J Clim 14:1337–1359

Hastenrath S (1984) Interannual variability and annual cycle: mechanisms of circulation and climate in the tropical Atlantic sector. Mon Wea Rev 106:1280–1287

Hastenrath S (1990) Decadal-scale changes of the circulation in the Tropical Atlantic sector associated with Sahel drought. Int J Clim 10:459–472

Hulme M (1994) Regional climate change scenarios based on the IPCC emissions projections with some illustrations for Africa. Area 26:33–44

IPCC (2001) Climate change 2001. The scientific basis. In: Houghton JT et al. (eds) Cambridge University press, Cambridge

Janicot S, Moron V, Fontaine B (1996) Sahel droughts and ENSO dynamics. Geol Res Lett 23(5):515–518

Johns TC, Gregory JM, Ingram WJ, Johnson CE, Jones A, Lowe JA, Mitchell JFB, Roberts DL, Sexton DMH, Stevenson DS, Tett SFB, Woodage MJ (2003) Anthropogenic climate change for 1860 to 2100 simulated with the HadCM3 model under updated emissions scenarios. Cim Dynam 20:583–612

Kalney E, Kanamitsu M, Kistler R, Collins W, Deaven D, Gandin L, Iredell M, Saha G, White G, Woolen J, Zhu Y, Chelliah M, Ebisuzaki W, Higgins W, Janowiak J, Mo KC, Ropelewski C, Wang J, Letmaa A, Reynolds R, Roy Jenne, Joseph D (1996) The NCEP / NCAR 40-year reanalysis project. Bull Amer Met soc 17(3):437–471

Kidson JW (1977) African rainfall and its relation to the upper air circulation. QJR Meteorol Soc 103:441–456

Lamb PJ (1978a) Large scale tropical surface circulation patterns associated with Subsaharan weather anomalies. Tellus 30:240–251

Lamb PJ (1978b) Case studies of tropical Atlantic surface circulation patterns during recent sub-Saharan weather anomalies: 1967 and 1968. Mon Wea Rev 106: 482–491

Lamb PJ (1983) West African water vapour variations between recent contrasting sub-Saharan rainy seasons. Tellus 30:240–251

Laval K, Picon L (1986) Effects of a change of the surface albedo of the Sahel on climate. J of atm Sc 43:2418–2429

Maynard K, Royer JF, Chauvin F (2002) Impact of greenhouse warming on the West African monsoon. Clim Dynam 19:499–514

Maynard K, Royer JF (2004) Effects of "realistic" land-cover change on a greenhouse-warmed African climate. Clim Dynam 22:343–358

Mitchell TD, Carter TR, Jones PD, Hulme M, New M (2003) A comprehensive set of high-resolution grids of monthly climate for Europe and the globe: the observed record (1901–2000) and 16 scenarios (2001–2100). Journal of Climate: (submitted)

Morcrette JJ (1990) Impact of changes to radiation transfer parametrizations plus cloud optical properties in the ECMWF model. Mon Wea Rev 118:847–873

Moron V, Philippon N, Fontaine B (2003) Skill of Sahel rainfall variability in four atmospheric GCMs forced by prescribed SST. Geol Res Lett 30(23):2221–2224

Paeth H, Hense A (2003) SST versus climate change signals in West African rainfall: 20th century variations and future projections. Climatic Change 65(1–2):179–208

Palmer TN (1986) Influence of the Atlantic, Pacific and Indian oceans on Sahel rainfall. Nature 322:251–253

Rowell DP (2001) Teleconnections between the tropical Pacific and the Sahel. QJR Meteorol Soc 127:1683–1706

Royer et al (2002) Simulation of Climate changes during the 21st century including stratospheric ozone. CR Geosci 334:147–154

Santer BD, Wigley TML, Barnett TP, Anyamba E (1996) Detection of climate change and attribution of causes. In: Houghton JT, Meira Filho LG, Callander BA, Harris N, Kattenberg A, Maskell K (eds) Climate change 1995. The science of climate change. Cambridge University Press, Cambridge, pp 572

Shinoda M, Kawamura R (1994) Tropical rainbelt, circulation and sea surface temperatures associated with the Sahelian rainfall trend. J Meteor Soc Jpn 72:341–357

Simons AJ, Burridge DM, (1981) An energy and angular momentum conserving vertical difference scheme and hybrid coordinates. Mon Wea Rev 109:758–766

Smith TM, Reynolds RW, Livezey RE, Stockes DC (1996) Reconstruction of historical sea surface temperatures using empirical orthogonal functions. J Climate 9:1403–1420

Sultan B, Janicot S (2003) The West African monsoon dynamics. Part I: documentation of intraseasonal variability. J Clim 16(21):3389–3406

Trenberth KE (1999) Conceptual framework for changes of extremes of the hydrological cycle with climate change. Climatic Change 42:327–339

Zheng X, Eltahir EA (1998) The role of vegetation in the dynamics of West African monsoon. J Clim 11:2078–2096